PHOTOMASK

BACUS—The international technical group of SPIE dedicated to the advancement of photomask technology.

EMLC 2012 Invited Paper 7985-17

Mask 3D effects: impact on Imaging and Placement

Jo Finders and Thijs Hollink, ASML, De Run 1110, 5503 LA Veldhoven, The Netherlands

ABSTRACT

In this paper we perform a fundamental study on the impact of mask absorber in ArF immersions lithography: the mask 3D effects. From simulations and analysis of diffraction coefficients we could identify a range of relevant features and imaging and placement phenomena. For these features, experimental results were obtained to pinpoint the mask 3D effects. We will demonstrate how to model and understand the mask 3D effects and give solutions to counteract the mask 3D effects.

1. Introduction

The impact of mask absorber geometry on wafer performance for ArF immersion lithography, socalled mask 3D effects, is attracting increasing R&D effort over the last couple of years. When memory makers were pushing lithography of the array like dense structures, the first noticeable effect was need of CD biasing to get the maximum aerial image contrast. This bias turned out to be different for different absorbers e.g. binary or attenuated phase shifting stack [1]. The next effect was a noticeable difference in best focus for various features. Theoretical ab initio calculations [2] revealed strong phase offsets in the diffracted orders, confirmed by other authors [3].

In this paper we will use a commercial simulator to extract the phase information from the diffracted orders to study the mask 3D effects. While the theoretical ab initio work is mainly

Continues on page 3.

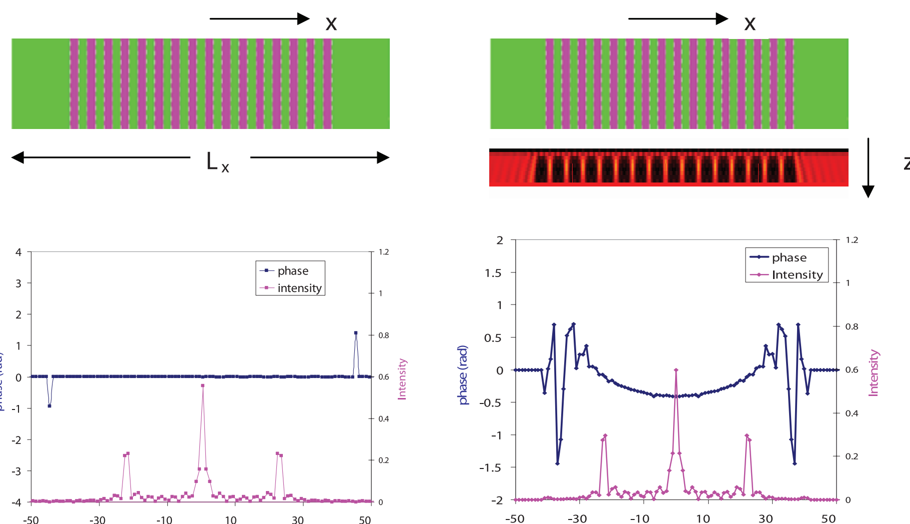

Figure 1. Top simulator set-up; grating domain size in x-direction and near-field image in case of rigorous simulation. Bottom: Phase and intensity of scattering coefficients for flat "Kirchhoff" case (left) and rigorous simulation (right). Diffracted orders are calculated for normal incidence, TE polarization.

Take A Look Inside:

Industry Briefs
—see page 16

Calendar
For a list of meetings
—see page 17

Editorial

I Wonder.

M. Warren Montgomery, *The College of Nanoscale Science and Engineering (CNSE)*

As summer begins to wind down, and the kids are focused on returning to school, the BACUS Steering Committee is gearing up for the 2011 Photomask Conference.

This year's conference chairs are Wilhelm Maurer and Frank Abboud. I approach the conference with great anticipation because this year we are joined by our colleagues from Photomask Japan for a Special Session on Monday afternoon. The early count of attendees is strong – up 18% as I write this – so I'm confident this will be a great conference.

At the conference, we will receive an update on the status of mask technology as it relates to many aspects of the mask industry. There are still a lot of questions that need to be answered and I look forward to hearing what the technical experts from the various companies will teach us.

For example, what are the latest results on the emerging and on-going issues facing the photomask industry? Will we receive an update regarding the recently delivered ASML 3100 tools? Have the recipients tested the validity of utilizing wafer level inspection as a methodology of verifying the quality of the pellicle-free EUV masks? And, what's the status of inspection tools for EUV masks?

One thing is certain: EUV will be one of the central topics addressed in a few months during the Advanced Lithography conference. Last year's talks (at Advanced Lithography) that focused on the new ASML scanners and the EUV sources were standing-room only. One wonders if e-beam lithography will be back in the discussion of future lithography technologies for semiconductor manufacturing, based on the recent findings reported in Microelectronic Engineering. I believe this meeting is ideally positioned to give a glimpse of the photomask-related "news to come."

As last year's President and Conference Chair, I would like to take this opportunity to encourage you to fill out the various survey forms that will be given to you by the SPIE team. These forms are a key source of guidance as to how the conference is serving you.

Beyond that, if you have suggestions for keynote speakers, special sessions, or how the conference could be improved, please share them with the conference chairs or any member of the Steering Committee, who are identified in your Photomask Conference program and in the monthly BACUS Newsletter. I must also take this opportunity to let you know that without your support, and that of your companies, this conference could not/would not happen.

In conclusion, I hope you share my enthusiasm as it relates to Photomask 2011. I am looking forward to rekindling prior relationships, firming existing relationships, and hopefully forging new relationships. I am looking forward to seeing you at the show, and possibly at the venue across the street (you know the place). Have a great conference; see you in Monterey.

N • E • W • S

BACUS News is published monthly by SPIE for BACUS, the international technical group of SPIE dedicated to the advancement of photomask technology.

Managing Editor/Graphics Linda DeLano
Advertising Teresa Roles-Meier
BACUS Technical Group Manager Pat Wight

■ **2011 BACUS Steering Committee** ■

President
Wolfgang Staud, *Applied Materials, Inc.*

Vice-President
Larry S. Zurbrick, *Agilent Technologies, Inc.*

Secretary
Artur Balasinski, *Cypress Semiconductor Corp.*

Newsletter Editor
Artur Balasinski, *Cypress Semiconductor Corp.*

2011 Annual Photomask Conference Chairs
Wilhelm Maurer, *Infineon Technologies AG*
Frank E. Abboud, *Intel Corp.*

International Chair
Naoya Hayashi, *Dai Nippon Printing Co., Ltd.*

Education Chair
Artur Balasinski, *Cypress Semiconductor Corp.*

Members at Large
Paul W. Ackmann, *GLOBALFOUNDRIES Inc.*
Michael D. Archuletta, *RAVE LLC*
Uwe Behringer, *UBC Microelectronics*
Peter D. Buck, *Toppan Photomasks, Inc.*
Brian Cha, *Samsung*
Kevin Cummings, *ASML US, Inc.*
Glenn R. Dickey, *Shin-Etsu MicroSi, Inc.*
Thomas B. Faure, *IBM Corp.*
Brian J. Grenon, *Grenon Consulting*
Jon Haines, *Micron Technology Inc.*
Mark T. Jee, *HOYA Corp, USA*
Bryan S. Kasprowicz, *Photronics, Inc.*
Oliver Kienzle, *Carl Zeiss SMS GmbH*
M. Warren Montgomery, *The College of Nanoscale Science and Engineering (CNSE)*
Emmanuel Rausa, *Plasma-Therm LLC.*
Douglas J. Resnick, *Molecular Imprints, Inc.*
Steffen F. Schulze, *Mentor Graphics Corp.*
Jacek K. Tyminski, *Nikon Precision Inc.*
John Whittey, *KLA-Tencor MIE Div.*

SPIE

P.O. Box 10, Bellingham, WA 98227-0010 USA
Tel: +1 360 676 3290 or +1 888 504 8171
Fax: +1 360 647 1445
SPIE.org
help@spie.org

©2011

All rights reserved.

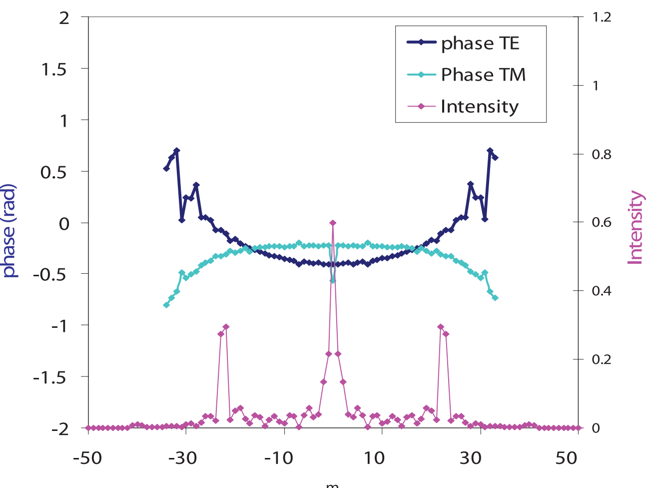

Figure 2. Comparison of scattering coefficients for TE and TM polarization under normal incidence. Grating and conditions as depicted in Figure 1. Rigorous simulation (FDTD)

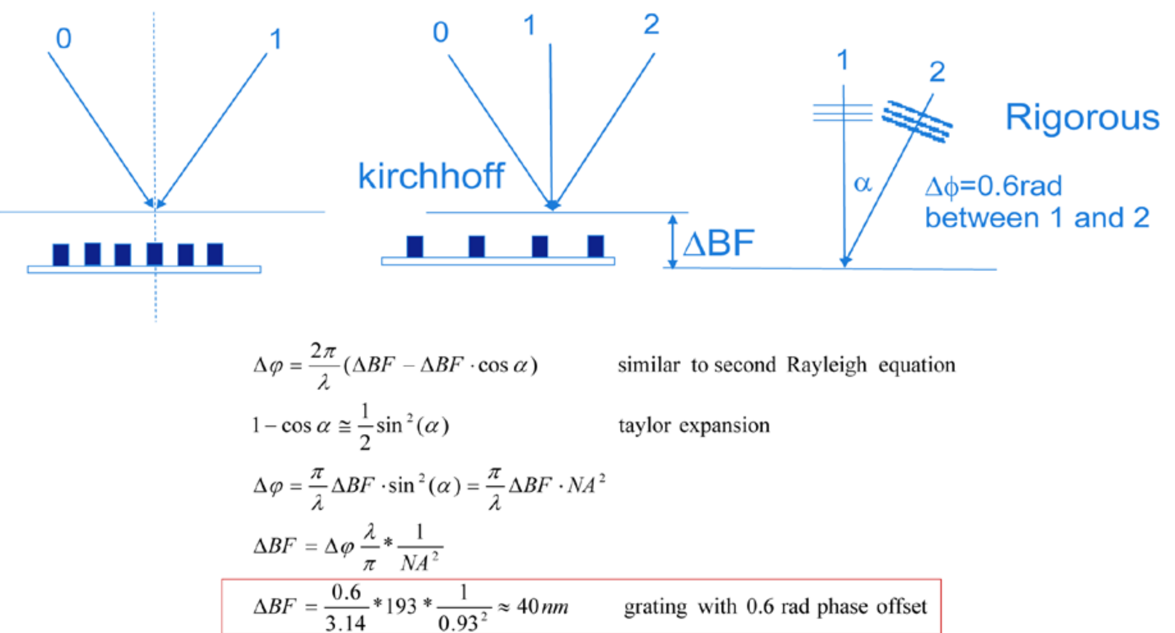

Figure 3. Analytic expression linking best focus difference and phase assignment due to mask 3D effect.

restricted to 1D gratings, we will study a wide range of patterns, all known to be relevant in past, current and future memory and logic designs. We will demonstrate that the impact of mask 3D effects goes beyond affecting only strength of the aerial image, also positioning errors will be studied and demonstrated.

In the first part we will give an explanation of the origin of mask 3D effects, studying the phase and intensity of the diffracted orders for a variety of patterns, predicting which effects we should be able to see on the wafer, if carefully studied. In the second part we will show experimental results and highlight which predicted effects we were able to capture on the wafer. In the next chapter we will study the strong impact of coherence setting on the observed phenomena attributed to mask 3D diffraction. As it will become clear that mask 3D effects are widely present and cannot be neglected, mask 3D aware simulation is required to optimize lithography. This holds for pre-tape out tasks such as scatter bar assignment during OPC and source mask optimization, as well as post-tape out tuning using advanced projection lens manipulators. The last part discusses methods to counteract the impact of mask 3D effects. The solution space here ranges from absorber optimization via design for manufacturing all the way up to application specific wave front tuning.

2. Explanation of the Mask 3D Effects

To explain the impact of mask 3D effects we will start with a simple grating with 45nm HP as depicted in Figure 1. All the simulations performed in this section are done assuming an attenuated Phase Shift Mask: different absorbers will be discussed later. All simulation to study phase assignments are done using the "Hyperlith" package [4]. In this package the scattering coefficients of the near-field image can be studied, before combining them in the projection lens. In the traditional "Kirchhoff" approximation

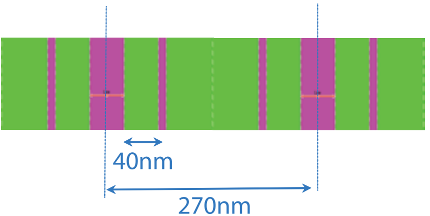

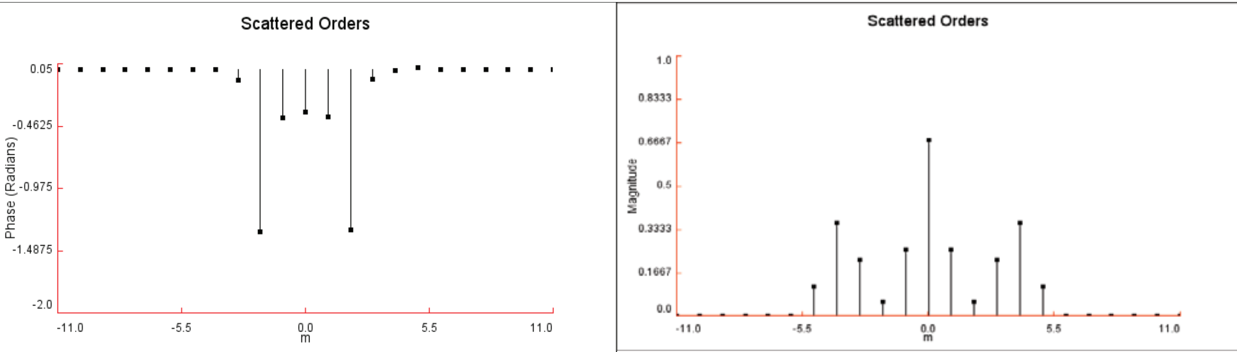

Figure 4. scattering coefficients for a main feature with small assist feature: main feature is 45nm, assist feature width equals 15nm, spacing between main feature and assist feature equals 40nm. Normal incidence, TE polarization. Pitch of main feature: 270nm (L_x=270nm in the simulator).

which treats the mask as a flat object, the Fourier transformation can be done directly from the mask transmission and phase. The scattering coefficients are calculated for a series of plane waves with wave vector:

$$k_x = m \bullet \frac{2\pi}{L_x} \quad m = \ldots, -3, -2, -1, 0, 1, 2, 3, \ldots \text{ etc.}$$

The scattering coefficients show only 0, π and $-\pi$ phase assignment. After removing the π and $-\pi$ offsets for visualization (see appendix), the phase and intensity are depicted in the left side of Figure 1. In the case of rigorous simulation, the near-field electrical field and image has to be calculated first. Performing a Fourier analysis on the rigorous calculated near field image yields the scattering coefficients in this case. After removing the π phase offsets for visualization (see appendix), the magnitude and phase of the scattering coefficients is plotted in the right side of Figure 1.

In the range of the diffracted orders ($-30<m<30$) the range of phase assignments equals 0.6 rad. This leads already to a important first conclusion: phase assignments due to stack geometry are in the order of 100 mλ (0.6 rad) and are thus much larger than the remaining lens aberrations in current projection lenses which are about 5mλ. To further demonstrate that these phase assignments are driven by mask stack properties, we compared the scattering coefficients for TE and TM polarization in Figure 2.

The opposite behavior of TE and TM is a clear indicator of the impact of mask 3D. The boundary conditions at the sidewall of the mask absorber are different for TE and TM polarization. The order of magnitude of observed TE-TM phase range in this work is in agreement with the phase range reported elsewhere [2,3]. The phase assignment in Figure 1b and Figure 2 is symmetric with respect to the optical axis k_x=0. For gratings with larger pitch the phase assignment is very similar, but shows more diffraction orders with non-vanishing intensity. For those pitches, the symmetrical phase assignment leads to a best focus difference. Using some simple assumption this best focus difference can be calculated analytically (illustrated in Figure 3). The derivation is very similar to the derivation of the second Rayleigh formula [5] and links phase assignment with (best) focus change. For a dense grating, under the conditions as shown in Figure 1, the grating is formed by two interfering waves (2-beam imaging). In this case the best focus shift is identical for both Kirchhoff and rigorous simulations, because of the phase symmetry. For a grating with pitch equals about two times the resolution limit, the situation is different (3 beam imaging). In this case 3-beam imaging occurs, which means there is a diffraction order close to the optical axis which will have a phase offset with respect to the orders from a high angle. This phase difference causes a shift in best focus (point with positive interference between the two waves). Assuming a phase difference of 0.6rad, the structure with pitch close to twice the resolution limit will have a best focus offset of 40nm compared to the grating at resolution limit. Note that the Taylor expansion used to derive the simple relation between Best Focus and phase is only valid for small NA (<0.5). Using the exact values would yield a BF difference of 70nm.

The strongest phase assignment so far amongst the structures we studied was not observed for simple L/S gratings but for structures with assist features (scatter bars). Figure 4 shows as an example the scattering coefficients of a 45nm structure with a 15nm assist feature, the space between the main feature and the scatter bar being 40nm at wafer level. Phase assignments up to 1.4rad are observed. It is very striking to observe a strong increase of phase assignment with decreasing space between main feature and assist feature. Figure 5 shows the phase of the scattering coefficients for spacing between main feature and scatter bar ranging between 30nm and 60nm. For spacing of 50nm and 60nm, phase assignments are moderate. The Bossung curves, as shown in lower half of Figure 5, is showing a normal frowning behavior and best focus is around -20nm. For spacing of 30nm and 40nm we see a very strong increase in phase assignments and the Bossung curves become tilted and skewed. Best focus (top of Bossung curve) is at +20nm ..+40 nm and becomes dependant on target CD.

This brings up a very interesting question: the definition of best focus for these kinds of tilted and skewed Bossung curves. From the point of view of CDU control, the top of the Bossung curve is a preferred working point, as focus errors have the least impact.

In the next step we are going to expand our analysis from a grating type structure to a structure for which the symmetry of the regular grating is broken by a space. Examples are the word

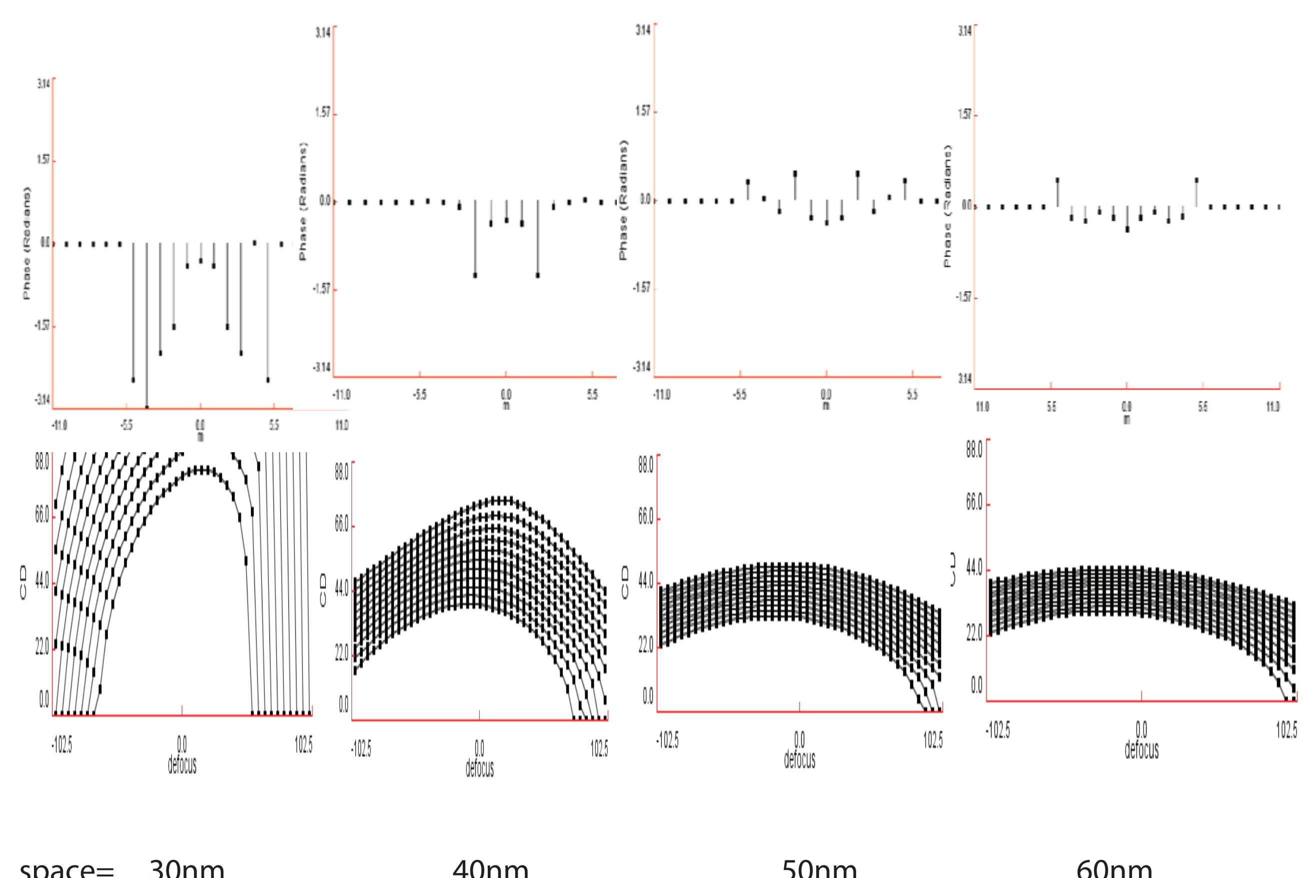

Figure 5. top row: scattering coefficient phase for different spacing between scatter bar and main feature. Scattering coefficients are calculated for normal incidence and TE polarization. Bottom row: aerial image Bossung curve for different spacing between scatter bar and main feature. From left to right: space=30nm, space=40nm, space=50nm and space =60nm. Dipole illumination 1.35 NA so/si=0.90/0.75, scattering coefficients for normal incidence. Structure as depicted in Figure 4.

lines of a Flash structure, a classical five bar or, in extreme, a two bar structure. For a two bar structure, mask 3D effects impact the imaging performance in a number of ways.

We first start examining this structure in a similar way as the grating before by judging the impact of the mask stack for normal incidence and TE polarization. Figure 6a shows the change of the phase scattering coefficients when increasing the MoSi thickness from nominal 68nm to 92nm. As expected a symmetrical phase change is observed. In current lithography, off-axis illumination is used to enhance the resolution limit. In Figure 6b the change in phase is depicted for an incident wave coming under an angle (For 1.35 NA and coherence σ at 0.9, this would correspond to an angle of 18 degrees). The delta phase profile is shifted towards negative values, with respect to k_x=0. A similar graph is shown in Figure 6c for the same negative incident angle. The delta phase profile is now shifted towards positive k_x values. When subtracting the two delta phase profiles in Figure 6b and 6c (plotted in Figure 6d) we observe a pure anti-symmetric profile.

For dipole illumination this means the following. The aerial image is formed by two aerial images created by the two incoherent poles. The two images are the same but are shifted with respect to each other. For a grating this leads to a fading of the aerial image and impacts Exposure Latitude and Mask Error Enhancement Factor. For a 2-bar structure this fading also leads to placement error since the aerial image of left edge and right edge of each line are different. This is illustrated in Figure 7a, were the actual aerial image for a two bar is plotted using the scattering coefficients from Figure 6. First observation is that the wafer pitch is smaller than the design pitch. This holds for both Kirchhoff and rigorous case. In the rigorous case there is an additional fading term due to mask 3D effect. This fading has more impact on the right edge of the left line than the left edge. Figure 7b shows the difference in pitch (wafer pitch- design pitch) for a range of design pitches and two illumination settings (annular and C-QUAD). This deviation from the design pitch up to 15nm has serious impact on lithography: the two lines are not positioned correctly on the wafer. This effect becomes pronounced for off-axis illumination. For small spaces the effect becomes up to 17nm.

The same holds for the end of an array: the outer features are shifted with respect to the middle part of the array. This is illustrated in Figure 8 for the word line structures of a Flash structure, a feature that is commonly used in Lithography.

So far all our considerations assumed the stack absorber to have a perfect rectangular profile. If this is not the case, the asymmetry of the absorber profile can translate into CD differences at the wafer level. To demonstrate this we again use the two-bar structure and assumed a very asymmetric profile. Again we fist looked into the scattering coefficients for different asymmetries and translated the differences in scattering coefficients into wafer CD results using the simulator. Figure 9 shows the scattering coefficients for two different absorber geometries (rectangular and skewed) under normal incidence and TE polarization: the phase assignment is symmetrical with respect to k_x=0. The phase profile for the skewed profile is not symmetrical anymore. When evaluating the difference

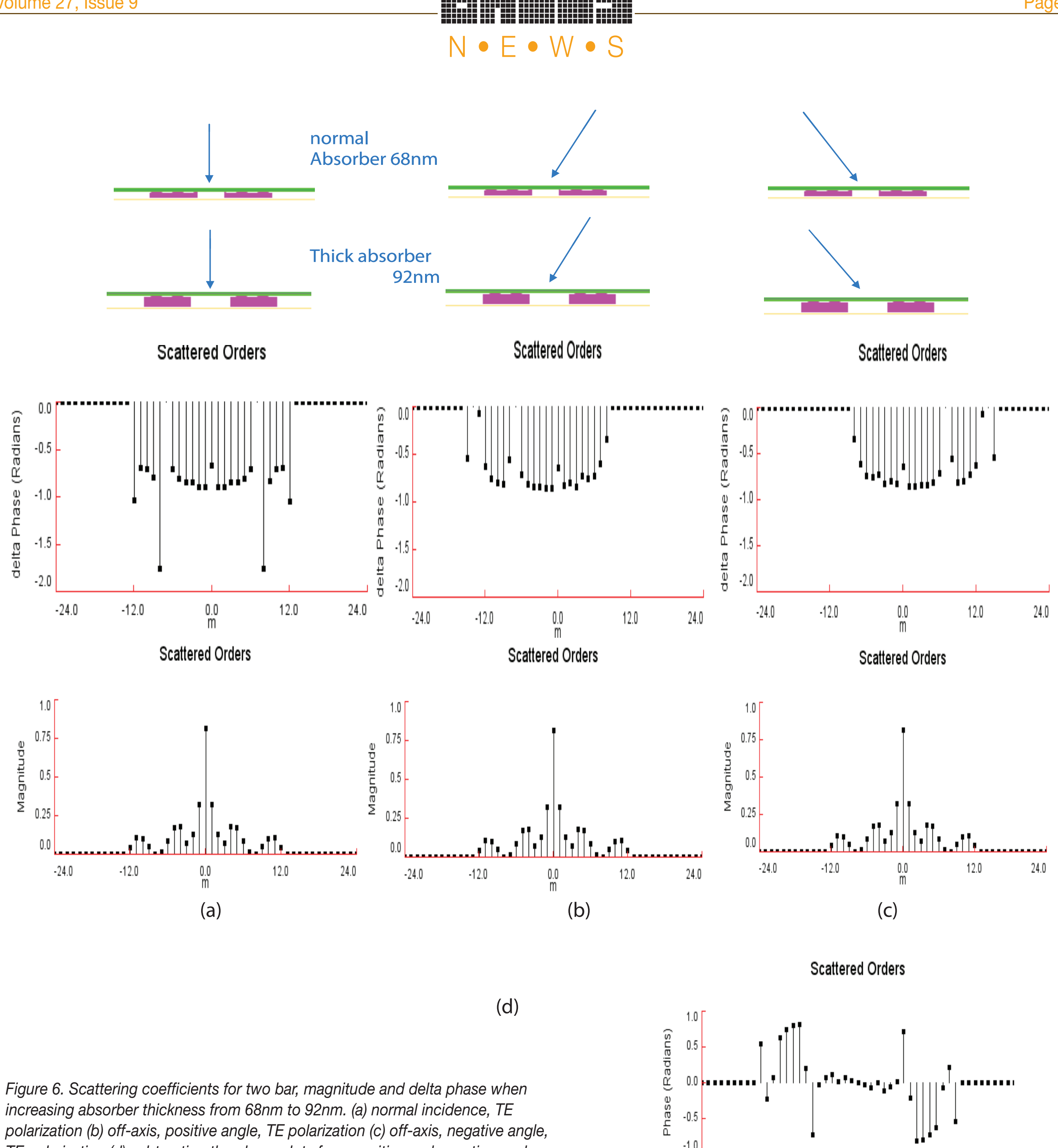

Figure 6. Scattering coefficients for two bar, magnitude and delta phase when increasing absorber thickness from 68nm to 92nm. (a) normal incidence, TE polarization (b) off-axis, positive angle, TE polarization (c) off-axis, negative angle, TE polarization (d) subtracting the phase plots from positive and negative angles (b)-(c)

of those two phase profiles (right column in Figure 9) a phase profile with odd symmetry is observed. The impact is expected to be very similar to that of odd lens aberration: although the two features are identical in the design and on the mask, on the wafer we expect a CD difference between the left line and right line.

This becomes visible in Figure 10: here the simulated L-R CD difference is plotted for a wide range of spaces in the 2-bar structure with skewed absorber profile. For small spaces, the difference in sidewall angle leads to an asymmetry in wafer CD, similar to the lens aberration. However, one distinct difference is observed: in the case of lens aberrations the CD-difference shows a second order behavior through focus (second order behavior due to bananicity of the aerial image). In the case the phase offset is caused at the mask side the behavior differs from the pure second order behavior. Figure 10 (b) shows the line asymmetry through focus for a 40nm space and skewed absorber profile. As can be seen the through focus behavior is almost constant. By changing the illumination setting in small steps, the through focus behavior changes from slight increasing CD difference through focus to constant through focus and even slightly decreasing CD difference through focus. Examining the through focus behavior of pattern symmetry is an effective way to discriminate between phase offsets created in the lens pupil and phase offsets created at the mask side.

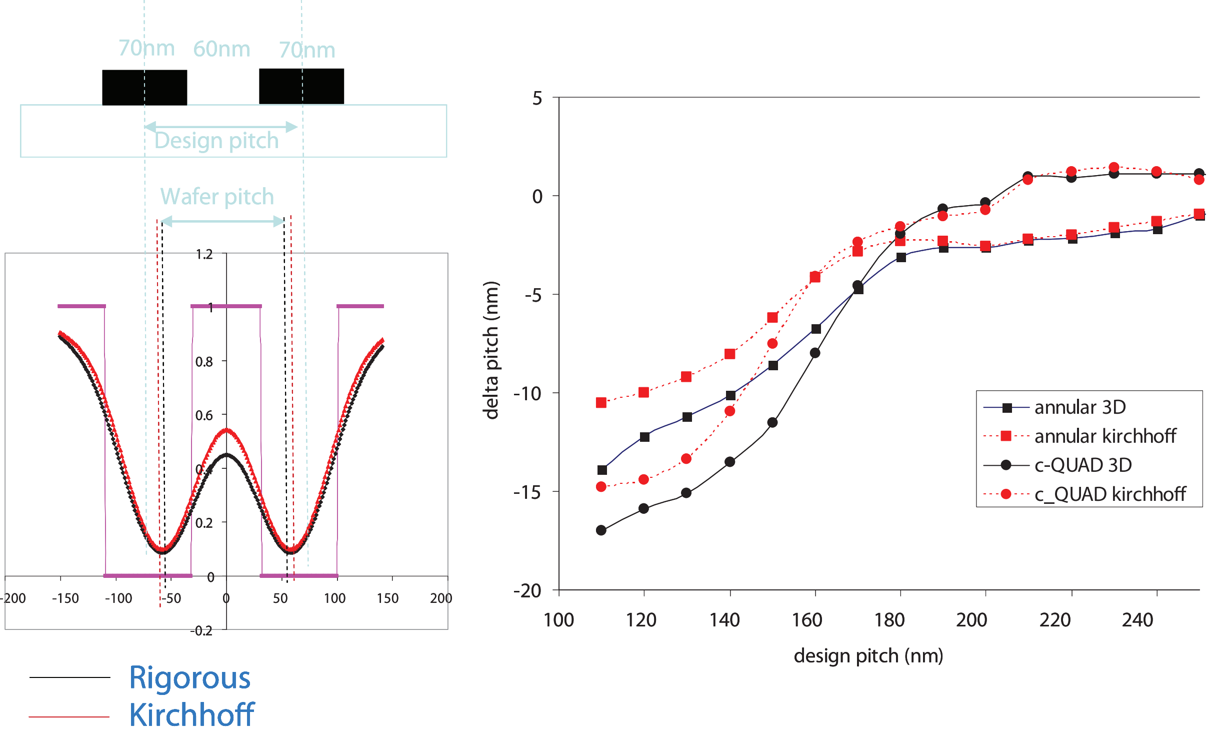

Figure 7. Left: 2 bar structure and aerial image ("rigorous and Kirchhoff"). Right: simulated difference between wafer pitch and design pitch for design pitches varying between 110 and 250nm.

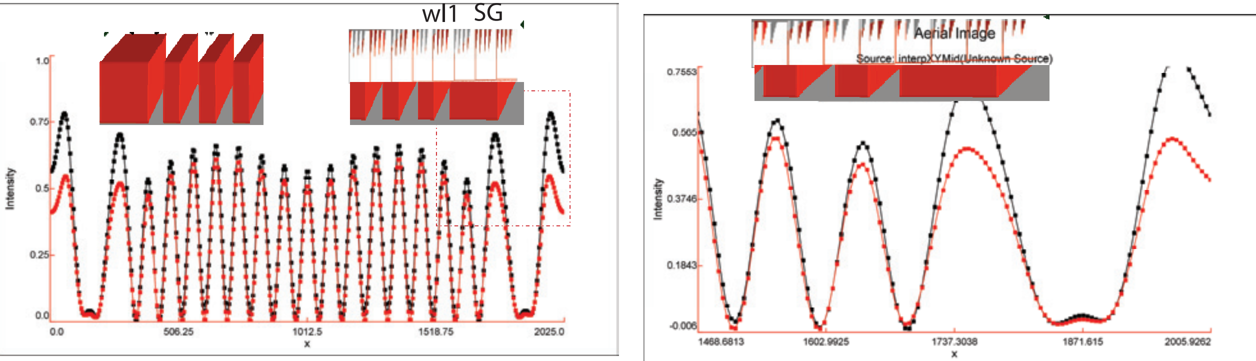

Figure 8. Left: rigourous (black curve) and Kirchhoff (red curve) simulation of Flash word line pattern (16 word lines wlx and Select Gate (SG). Right: zoom in into the right end of the array, clearly indicating a displacement of wl1 and SG when comparing rigorous and Kirchhoff simulation.

3. Experimentaly Observed Mask 3 Effects

In this and the next section, we experimentally studied the structures from the theoretical introduction on the mask 3D phenomena. All results are obtained using a MoSi attenuated PSM. The best focus differences between features are the easiest to observe [6]. Figure 11 shows the best focus difference for a variety of structure. The first 5 features are horizontal grating through pitch (preferred for the dipole illumination in y direction), the last two structures are vertical gratings. Features with 270nm and 315nm pitch have 1 or 2 scatter bars. Best focus in this experimental section is always extracted as top or bottom of a second order polynomial fit to the CD through focus curve. The experimentally observed best focus difference across the 7 features is 31nm and thus contributing significantly to the focus disturbances in lithography.

The next feature we investigated was the 2bar structure with varying space. Fist of all we measured the pitch of the structure on the wafer with CD-SEM and compared the values to the design pitch. Results are graphed in Figure 12 for both annular and C-QUAD illumination. As the space of the 2 bar decreases, a significant pinch of the structure occurs and the wafer pitch becomes much smaller than the design pitch. This holds for both annular and c-Quad illumination, however for c-QUAD illumination, it occurs already at much larger pitches.

The trend of delta pitch versus space is picked-up in the simulator for both rigorous and Kirchhoff approaches. However, the magnitude is only comparable when doing the simulations in rigorous mode. To correctly print the two-bar at small spaces OPC has to be performed to correct the CD due to classical OPE errors and edge place adjustment to place the lines correctly.

The last type of CD anomaly that was studied is the pattern

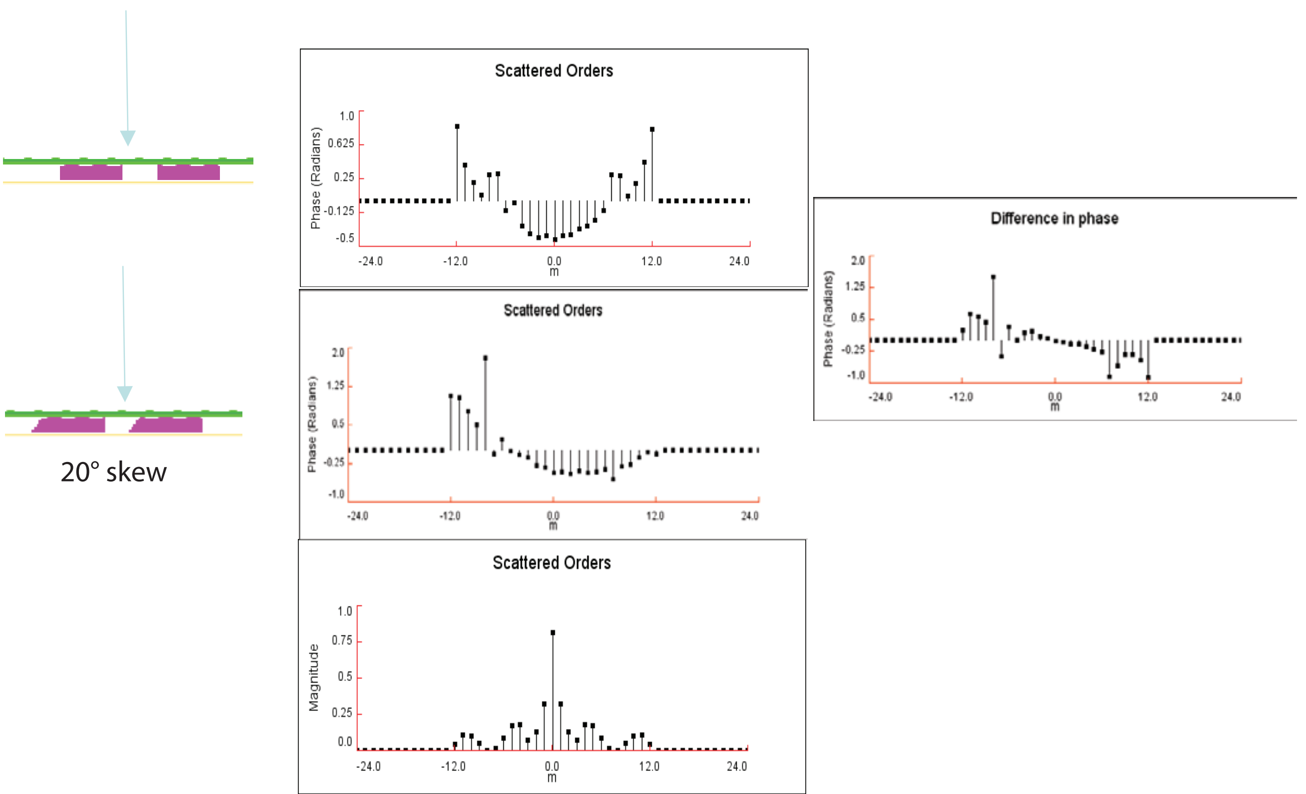

Figure 9. Comparison of scattering coefficient for 2-bar structure with rectangular absorber profile and skewed absorber profile. Middle column from top to bottom: phase of scattering coefficients for rectangular profile, phase of scattering coefficients for skewed profile: magnitude of scattering coefficients. Right column: difference in phase of scattering coefficient for rectangular and skewed profile.

asymmetry between left last line and right last line of 2bar, 5 bar and flash pattern. This was the most difficult parameter to measure experimentally: as the CD differences are only 2..3 nm, a lot of averaging was required. For the word line pattern of a Flash structure we consistently saw an offset in the CD between the top feature and the bottom features. A typical example is shown in Figure 13a. The two adjacent features SG and wl1 have opposite pattern asymmetry, this points towards a phase error as root cause. Furthermore the pattern symmetry was almost constant through focus, as shown in Figure 13b. The focus dependence changed when varying the coherence setting around the nominal coherence setting (σ_o/σ_i=0.91/0.75). For SG, we observed slight decrease of pattern asymmetry through focus at lower coherance values (σ_o/σ_i =0.77/0.62), constant pattern asymmetry through focus at nominal setting and slight decrease of pattern asymmetry through focus at higher coherance values (σ_o/σ_i=0.98/0.83).

All our observations strongly point towards odd phase errors introduced at the reticle side, potentially caused by Mask 3D in the case of an asymmetric profile. However, profile information is not readily available during the manufacturing process. Furthermore our test masks are running for an extended period (2 to 3 years). Contamination and cleaning might have deteriorated the initial absorber profile. At this point in time we conclude that we have pattern asymmetries, caused by a combination of residual lens aberration, reticle writing errors and mask 3D effects. In the last chapter we will look into ways to mitigate the pattern asymmetry.

4. Interaction of Mask 3D Effects and Illumination

Illumination setting optimization is one of the most important pillars of current resolution enhancement techniques [7,8]. Traditionally when this is done, mask 3D effects are not taken into account. In this section we investigated the coherence setting dependence of two pronounced mask 3D effects namely best focus difference per feature and edge feature placement. All results are experimental values. Fist we looked into the change of best focus per feature for different illumination settings (Figure 14). The dipole illumination setting was changed in very small steps ($\Delta\sigma_o/\Delta\sigma_i$=0.04).

Sine the minimum pitch is 45nm and up, operating at 1.35NA we are not close to the resolution limit and changing the illumination setting is a good way to probe the diffraction characteristics. Methodology is similar as explained in section 3 for Figure 11. For some features the best focus stays constant through illumination setting. The features that respond most are gratings at pitch 270nm and 315nm, both having scattering bars. For the feature at 270nm pitch, the best focus changes 15nm per 0.07σ. Therefore there is reason to use mask 3D aware modeling in the source mask optimization and/or the scatter bar assignment during OPC.

Conclusion and Outlook

Besides the best focus differences we studied the edge feature placement of a flash word line pattern under different illumination setting (Figure 15) The feature placement was determined as follows: SEM micrographs and measurement were obtained from wafers for the different illumination settings. From the SEM measurements the position of each feature was determined with reference to the middle feature and compared to its nominal design value. This deviation, called feature displacement was split in two parts:

- Features of the top part and bottom part move in opposite direction towards the center line of the flash pattern. Features stay symmetric with respect to center axis. Root causes are classical Optical Proximity Effect and Mask 3D fading effect as demonstrated in section 1
- Features of the top part and bottom part move in the same direction. Features are asymmetrically placed with respect to center

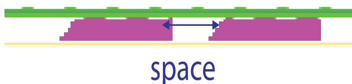

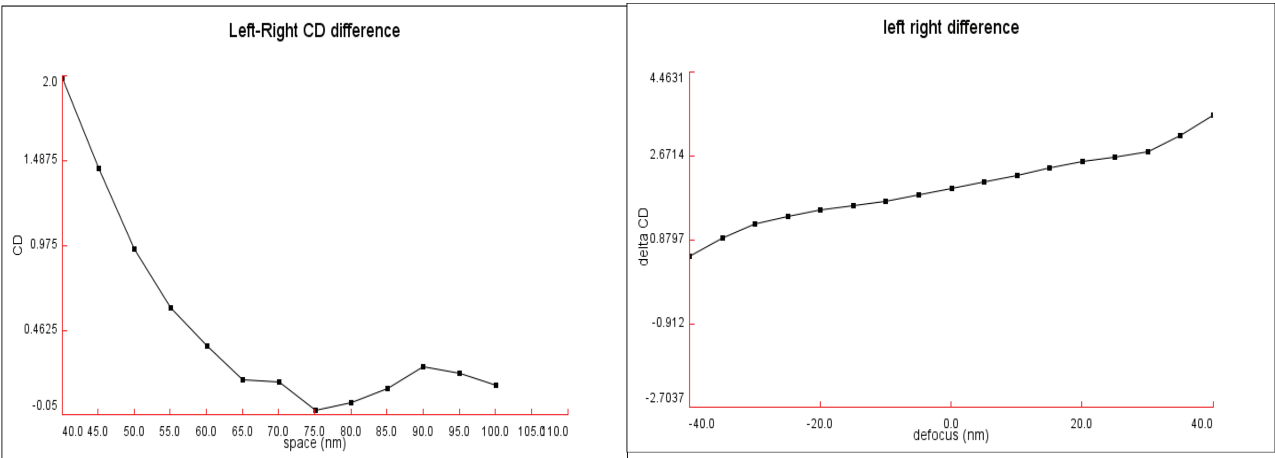

Figure 10. Left graph simulated left-right difference for a skewed absorber profile for a range of spaces of 2-bar pattern: design line CD is 70nm, 1.2NA, C_QUAD illumination, σ_o/σ_i=0.97/0.77, TE polarization. Right graph: for space equals 40nm: pattern asymmetry through defocus.

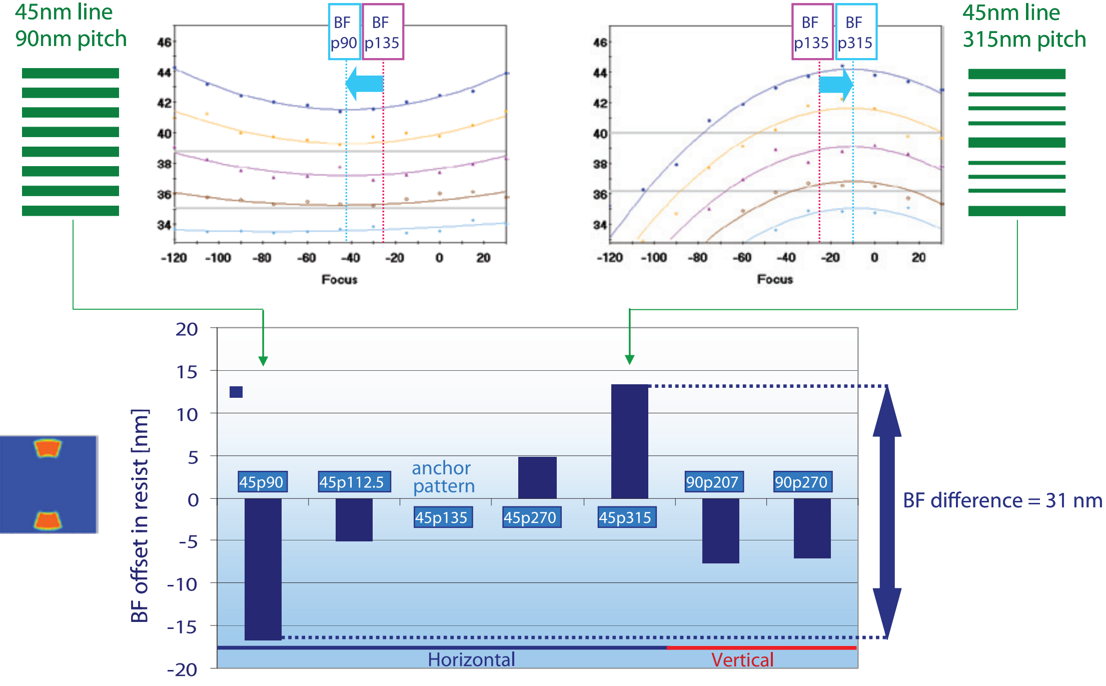

Figure 11. Top: Bossung curves and fitted polynomial (solid lines) for two features. Bottom: fitted best focus through feature type. Dipole illumination, σ_o/σ_i= 0.98/0.83, NA=1.35, TE polarization.

axis. Root cause are classical odd lens aberration and mask 3D errors (odd aberrations in case of asymmetric sidewall angle)

The biggest effect experimentally observed is a symmetric displacement of the edge features. For SG the displacement is 2nm per 0.07σ change in coherence setting.

5. Modeling capability

For future nodes were (sub) nm tolerances are required on placement and Critical Dimension control, mask 3D effects will need to be taken into control at all stages of lithography simulations. This requires simulation tooling which can go beyond clip level approach like in section 1 to a fast and accurate full chip modeling. Figure 16 shows the comparison between the experimentally observed best focus difference and the simulated best focus difference using Tachyon™ M3D. Excellent agreement between simulation and experiment has been achieved with a linear regres-

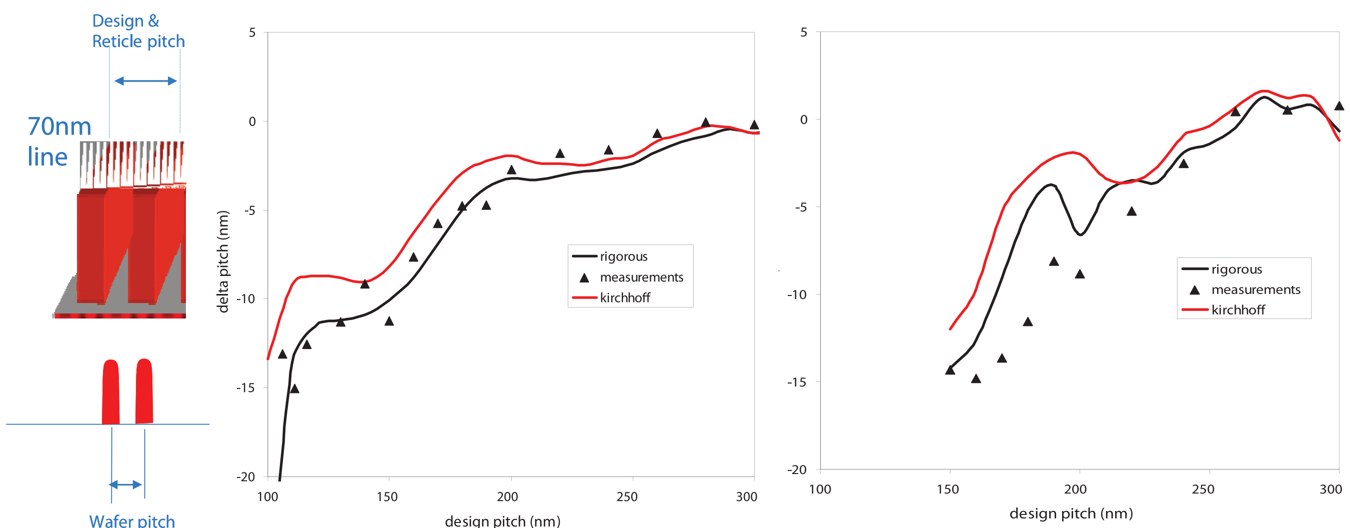

Figure 12. Top: Deviation between design pitch and wafer pitch for 2 bar structure with various space width. Left graphs are for annular illumination, right graphs are for c-QUAD illumination. 1.2 NA σ_o/σ_i =0.97/0.77.

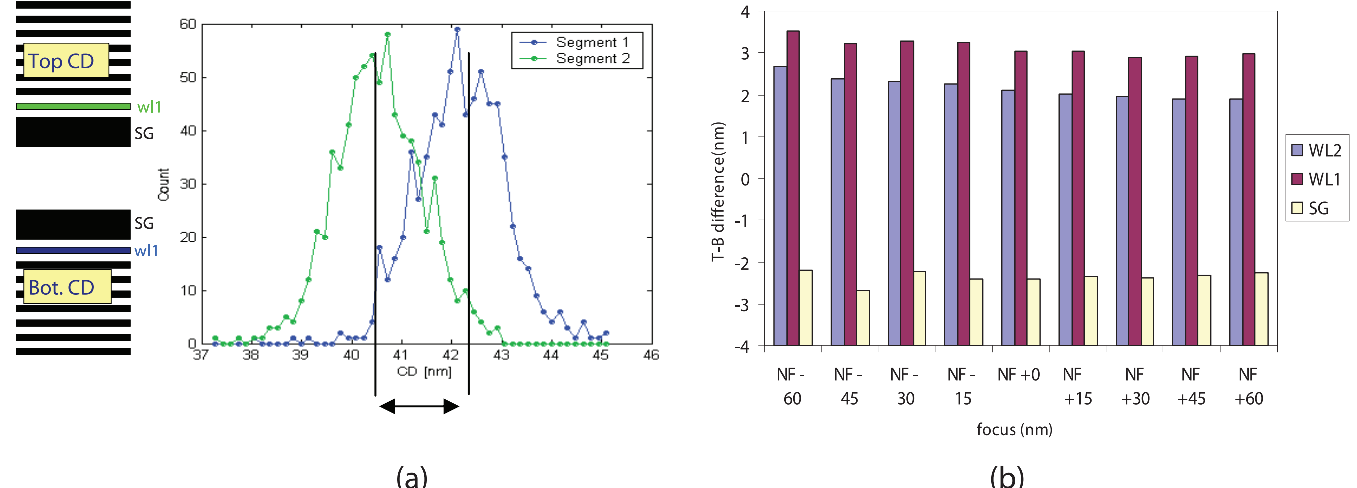

Figure 13. (a) wafer CD histogram for wl1 located in the upper part of the Flash pattern and the corresponding wl1 (blue curve), in the lower part of the Flash pattern. 1.35 NA dipole illumination s0/si=0.91/0.75 (b) through focus behavior of the pattern assymetry.

sion coefficient of 0.99 and R2 of 0..94. This end result has only been achieved after optimizing and tweaking the physical model in the simulator.

Next step will be to gain the same kind of accuracy on figure of merit like edge feature placement and pattern asymmetry. Especially the last one will require the incorporation of mask profile information into the simulator. Most simulators can handle mask geometry profiles beyond a simple rectangular profile. Future work is required to establish if and what kind of profile information needs to be inputted into the simulator.

6. Handling of the Mask 3D Effects

As it becomes clear form the previous chapter, mask 3D effects manifest themselves in many different ways and cannot be ignored, especially if a plurality of features needs to be printed at the same time. The first and most intuitive way is to optimize the absorber material. Alternatives to MoSi attenuated stack have been proposed: binary and OMOG. Different absorbers come with different n and k values and influence the boundary conditions at the sidewall for TE and TM incident light. This optimization has been very effective for aerial image contrast of a single grating[1].

In case we are considering a plurality of features or multiple figures of merit trade-offs have to be made:

For the best focus differences per feature no significant improvements were observed in simulations of various mask stack materials. Some pitches show best focus differences; others are almost not affected (compare to Figure 11, 14 and 16 for attenuated PSM). These critical pitches change for different absorbers and in order to make a fair comparison the full parameter space (through pitch, through size, etc.) has to be covered, dependant on the application. The most effective parameter to reduce the effect is reducing the absorber height. However, compared to our reference MoSi stack of 68nm height, a significant reduction is required (factor 2 or more) which would have severe detrimental side effects (low aerial image contrast). We plan future work to quantify the lithography effects as explained in the theoretical and experimental part for different absorbers.

Once a given absorber is chosen, mask 3D effects can be

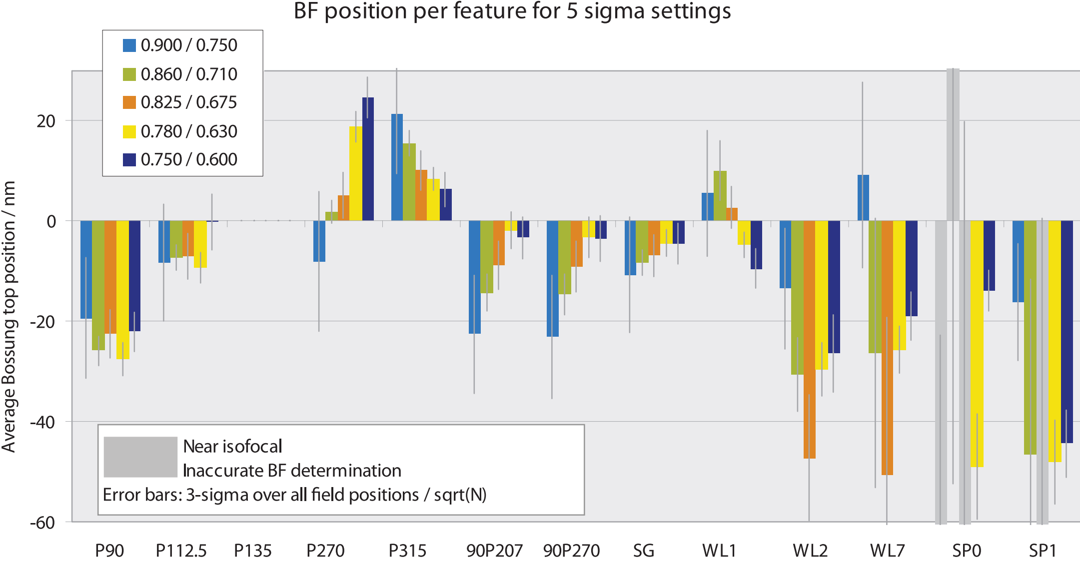

Figure 14. Experimental best focus through feature for five different dipole illumination setting. 1.35 NA. First 5 features: through pitch gratings preferred direction of the dipole (ref. Figure 11). Next two features: through pitch grating, non-preferred direction of the dipole (ref. Figure 11). Last features: Flash word line structures (ref Figure 8 and 13).

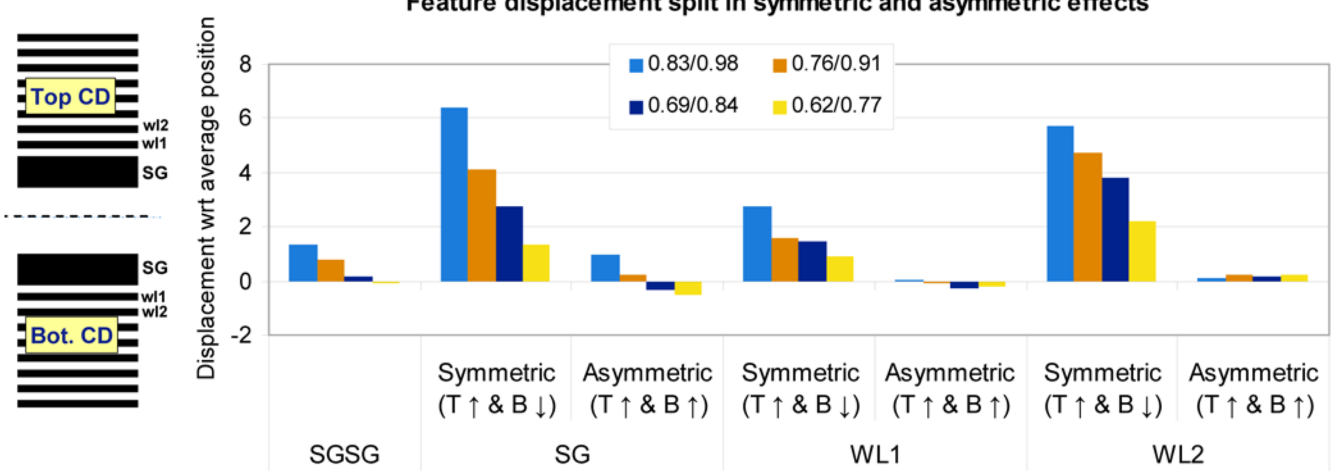

Figure 15. Feature placement change under various illumination conditions. Experimental measurements bases on CD-SEM. 1.35NA, dipole illumination TE polarization. SGSG: space between the two SG features.

handled in a variety of ways both pre-tape out; before the creation of the reticle and post-tape out; compensating the wafer impact for a given reticle. A prerequisite of full chip mask 3D modeling as explained in the previous section holds for any of these techniques:

- Design for manufacturing (pre-tape out)
- Mask 3D aware Source Mask optimization. (pre-tape out)
- Mask 3D aware Source Mask and phase optimization (pre-tape out)
- Tuning residual wafer effects by an application specific wave front (post-tape out)

During the design of the chip the layout of the chip can be optimized to be the least susceptible for mask 3D effects. Figure 17 shows an example for Flash word line patterns. For the left layout, after OPC we observe a pattern asymmetry for SG of -1.5nm for the attenuated absorber stack and -0.5nm for the binary stack. Pattern asymmetry is constant through focus, pointing towards phase errors as a potential source. Please note that binary and absorber parts are on the same reticle, and that wafer CD is same for both absorbers after their respective OPC. From this one might judge the binary stack to be better performing. However, when slightly modifying the design layout, the pattern asymmetry is reversed and the same value of around +1.5nm was achieved for both binary and attenuated PSM stack. Obviously, by changing the design layout the pattern asymmetry is also influenced. Key parameters are the size of the two adjacent spaces next to SG (SGSG and sp0). This is not surprising as in section 1 it was shown that strong phase assignment are associated with small changes in space dimension. For a space ratio (SGSG/sp0) of 4 we observed a negative pattern asymmetry, for a space ratio of 3 we observed a positive pattern asymmetry.

Once the design is fixed as well the basic diffraction pattern is fixed and can only be changed within certain limitations (scatter bars and feature biasing). This leads to a certain phase assignment which can have detrimental effects in wafer lithography as

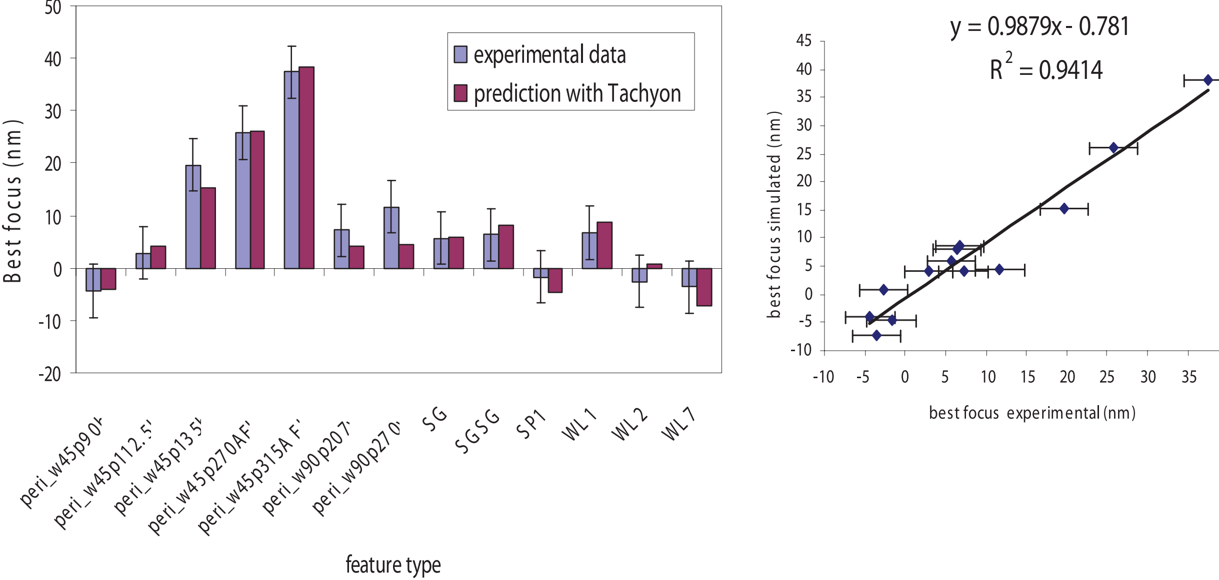

Figure 16. correlation between experimentally determined best focus and best focus simulated with Tachyon™ M3D. Experimental condition: same as in Figure 11.

explained in the first two sections. It is very natural to counteract the impact on phase by mask 3D effects by an application specific wave front which can be applied in the projection optics. We developed a way of introducing a high order phase profile of the wave front (Flexwave [6]). The spatial frequency, in terms of a Zernike expansion order goes beyond the traditional number of 36. Details will be explained elsewhere [9]. Of course the range of the phase correction to steer the imaging has to be larger than the current residual after lens setup.

In this way, an application specific wave front can compensate the best focus differences between features for gratings through pitch and word line structures of Flash layout [6]. Since most of our test masks containing a Flash word line pattern also show a pattern asymmetry, we optimized the application specific wave front to compensate best focus differences and pattern asymmetry simultaneously.

The outcome of this optimization is shown in Figure 18, before and after optimization and applying the application specific wave front. First, we tried to correct the observed pattern asymmetry for the various features of a Flash pattern (top row Figure 18). An asymmetric phase profile was applied and could reduce the pattern asymmetry by more than 50%, as verified by wafer results. The fact that the phase assignment improves all features is a further indication that the origin lies in a phase error. Secondly we tried to correct for the best focus differences for gratings through pitch and the structures of the Flash structure (middle row Figure 18). Applying a more symmetric phase front could reduce best focus differences by 50%

Dipole illumination (vertical orientation). 1.35 NA, TE polarization. Experimental data measured with CD-SEM.

Finally, we tried a simultaneous correction of best focus differences and pattern asymmetry (bottom row, Figure 18). The combined application specific wave front is shown in the bottom of Figure 18. For both pattern asymmetry and best focus asymmetry we observe an improvement of 50%! This type of correction needs a holistic lithography approach with advanced wave front manipulation capabilities on the scanner and strong computation aspects. For the computational side the main requirement is a full chip simulator which can handle the mask 3D effects as accurate as demonstrated in Figure 16. Beyond this we have multiple complicated litho metrics (best focus and pattern asymmetry) with interactions for a plurality of features, which cannot be handled anymore by simple sensitivity based linear optimization.

7. Conclusions

In this paper we have demonstrated by means of simulation and experimental verification a number of imaging effects that occur due to the finite thickness of the absorber stack on the mask in ArF immersion lithography ("Mask 3D effects"):

- Focus variations between features in the order of 40nm.
- Pattern asymmetry between edge features of 2-bar, 5-bar and Flash pattern. The left and right feature could differ by 3nm in CD in case the absorber profile is not symmetric (i.e. left sidewall angle and right sidewall angle are different).
- Placement error for edge features of 2-bar, 5-bar and Flash pattern. The edge features are shifted 3nm with respect to the inner features due to mask 3D effects.

The effects become pronounced when polarized light is used. For hyper NA and a half pitch below 50nm these effect are becoming visible in wafer lithography. For the 22nm node the magnitude of the effects becomes large compared to process window and CDU requirements. Control of CD and placement errors due to mask 3D are crucial for the extension of ArF immersion lithography to 22nm and below.

Mask 3D effects and its impact are very similar to the impact of lens aberrations. This was revealed be a study of the phase of the scattering coefficients. One main difference is that they are created at the object side and thus have a different through focus behavior. We observed even and odd phase offsets in the scattering coefficients attributed to mask 3D effects. The phase contribution from the mask 3D can be as large as 100mλ and is thus larger then the residual lens aberrations which are 5mλ or smaller.

There is a strong interaction of the mask 3D effects with the design layout. For features with scatter bars we observed a large phase assignment and best focus offset when the space between main feature and scatter bar becomes 40nm. For a flash structure the observed pattern asymmetry could be mitigated by carefully designing the spaces between the structures.

There is also a strong interaction with the illumination setting: for some features the mask induced effects change drastically

Layout case1

Waferlevel	
Feature	Mod 10: 39
SGSG	185
SG	162
SP0	45
WL1	35
SP1	43
WL2	33
WL7	39

Layout case2

Waferlevel	
Feature	Mod 14: 40
SGSG	202
SG	148.25
SP0	69
WL1	49
SP1	42.25
WL2	33
WL7	40

Figure 17. Experimentally observed pattern asymmetry for SG pattern in Flash word line structure for two different layout case and two different absorbers (binary and attenuated). Absorber details are explained in reference [1].

with small change in coherence setting. For gratings with scatter bar we observed a 15nm change of best focus with only 0.07 change in coherence setting. For the edge features of a flash word line pattern we observed a 2nm placement difference for a 0.07 change in coherence.

As a way to compensate the impact we propose the application of phase with opposite sign as created by the mask 3D effect. This requires the combination of advanced wave front manipulation capabilities on the scanner and strong computational aspects. On the scanner we implanted the possibility of high order phase assignment in the projection pupil to counteract mask 3D effect. On the computational side we enable full-chip capabilities to accurately predict the best focus differences due to mask 3D effects. Applying a high order optimum phase profile, calculated by computation across a variety of feature we were able to reduce pattern asymmetry and best focus differences at the same time by 50%.

Similar phenomenological effects can be expected for future lithography using EUV masks. In the near future we will expand this work and methodology by looking at EUV lithography.

8. Acknowledgment

Mircea Dusa and Eelco van Setten for designing the mask layout and gathering experimental results to study the absorber impact on pattern asymmetry.

Tom Pistor for extensive discussions; for enabling this fundamental work through his software package and for fast adaptation of the software whenever needed (the skewed profiles).

Peng Liu, Paul van Adrichem for simulations of best focus difference using Tachyon modeling.

Brid Connelly, Marcus Bender and Martin Sczyrba (AMTC) for fruitful discussions on mask absorber geometry.

Jan Willem Gemmink, Judith van Praagh, Dorothé Oorschot, Sander de Putter, Kees GrimFrensly Vlijt, Yin Fong Choi, Bambang Asmowidjojo and Wendy Liebregts for creation of a million data points. Without the help of this team we would never be able to pick up some of these small CD effects (1 to 2nm or less).

9. Appendix

When studying and visualizing the scattering coefficients, the phase assignment very often looks as depicted in Figure 19a. There are two groups of phase assignment, which are offset by π.

In fact, when closely examining each pair of plane waves with wave vector $+k_x$ following relation is observed:

For wave vector with k_x: phase equals ϕk

For wave vector with $-k_x$: phase equals $\phi k + \pi$

The offset between the two groups can be removed. E.g.: for each pair of wave vectors $(+k_x, -k_x)$ π is subtracted from the phase of one of the plane waves.

For wave vector with k_x: phase equals ϕk

For wave vector with $-k_x$: phase equals ϕk

The results after correcting the phase pair wise, is shown in Figure 19b.

These two are equivalent for visualization, the addition of the individual plain waves will lead to the same aerial image of opposite tone.

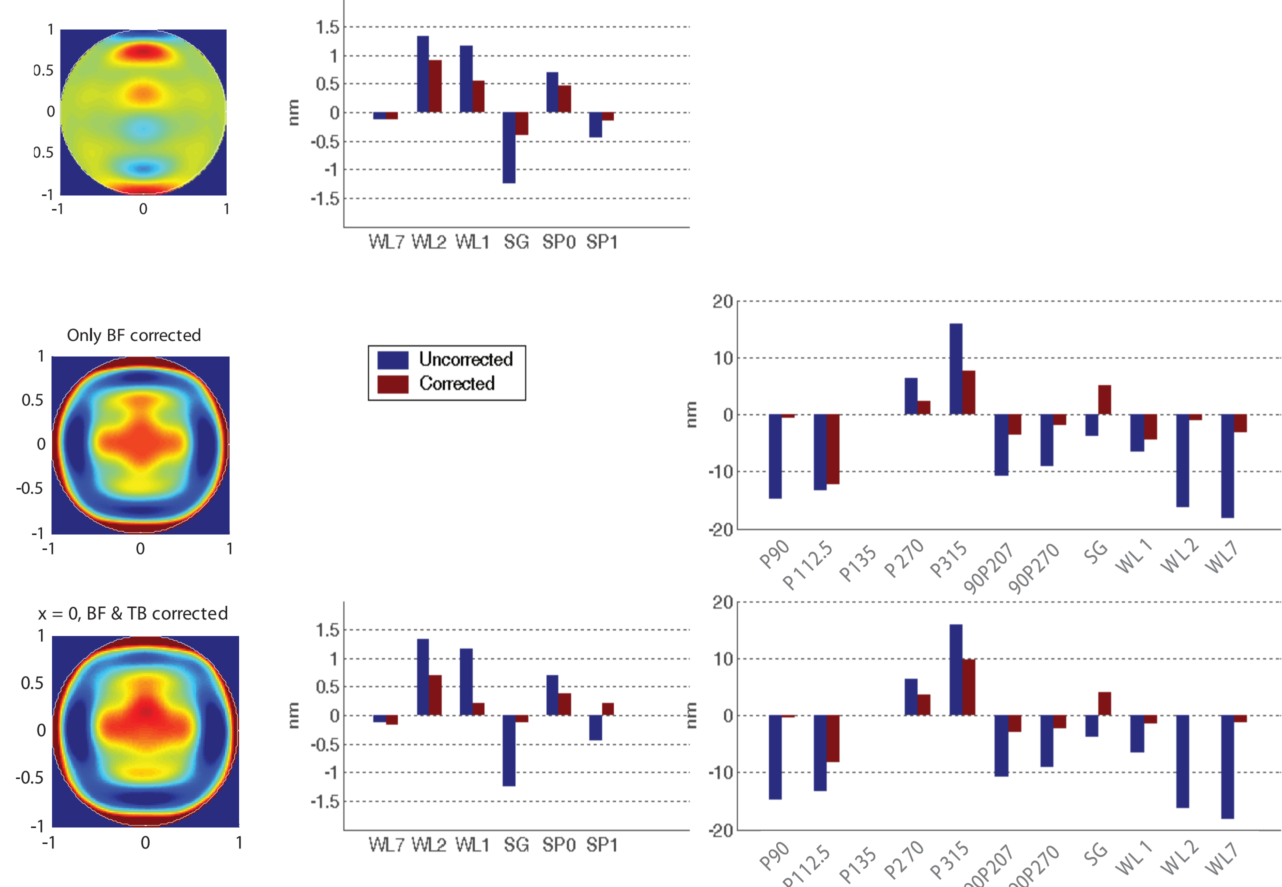

Figure 18. Applying an application specific wave font to correct pattern asymmetry and best focus differences. Top row: applying wavefront to correct for Pattern assymetry of various structures of Flash pattern. Middle row: applying application specific wavefront to coorect for best focus differences of gratings through pitch and Flash structures. Botton row: applying application spefic wavefront to simultaneously correct for best focus differences and pattern assymetry.

10. References

[1] Eelco van Setten, Andre Engelen, Jo Finders, and Mircea Dusa, "Masks for flash memory gates for the 45nm node: binary or attenuated?" Proc. SPIE 6533 (2007).

[2] Johannes Ruoff, Jens Timo Neumann, Emil Schmitt-Weaver, Eelco van Setten, and Nicolas le Masson, Chris Progler, Bernd Geh: "Polarization-induced astigmatism caused by topographic masks Proc. SPIE 6730 (2007).

[3] A. Erdmann, F. Shao, P. Evanschitzk, and T. Führer, "Mask-topography-induced phase effects and wave aberrations in optical and EUV lithography", Journal of vacuum science and technology. B, microelectronics and nanometers 28.2010, Nr.6.

[4] www.panoramictech.com

[5] Kurt Ronse PhD thesis, "Phase shifting masks for optical lithography: principles, manufacturing and imaging performance" IMEC, 1994.

[6] Jo Finders, Mircea Dusa, Peter Nikolsky, Youri van Dommelen, Robert Watso, Tom Vandeweyer, Joost Beckaert, Bart Laenens, and Lieve Van Look, "Litho and patterning challenges for memory and logic applications at the 22-nm node", Proc. SPIE 7640 (2010).

[7] Jo Finders, Louis Jorritsma, Mark Eurlings, Richard Moerman, Henk van Greevenbroek, Jan B. van Schoot, Donis G. Flagello, Robert J. Socha, and Thomas Stammler "Can DUV take us below 100 nm?" Proc. SPIE 4346 (2001).

[8] Robert Socha, Xuelong Shi, and David LeHoty, "Simultaneous source mask optimization (SMO)" Proc. SPIE 5853 (2005).

[9] Frank Staals et al., "Advanced wavefront engineering for improved imaging and overlay applications on a 1.35 NA immersion scanner", Proc. SPIE 7973 (2011), to be published Proc. of SPIE Vol. 7985 79850I-23.

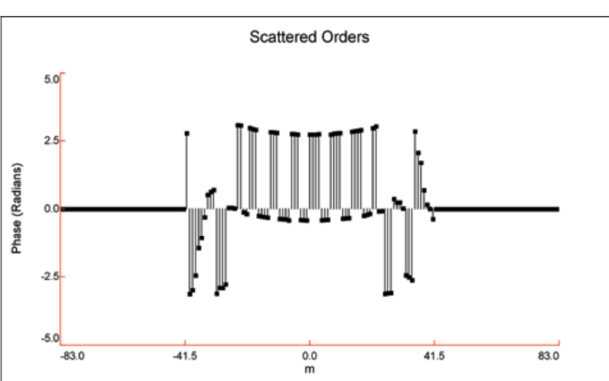

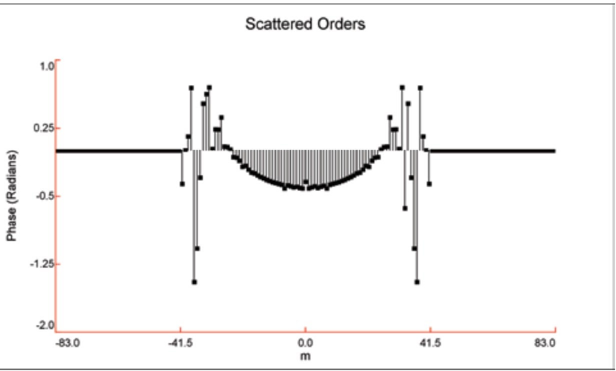

Figure 19. Left: phase assignment in diffracted orders, raw output from hyperlith. Right: phase assignment for visualization after applying offset of -π for one of the waves in the pair (k_x, $-k_x$)

Original:

$$\vec{E}_k = \cos(kx + \phi_k) + \cos(-kx + \phi_k)$$
$$= 2 * \cos(\phi_k)\cos(kx)$$
$$I = \sum_k 4\cos^2(\phi_k)\cos^2(kx)$$

For visualization:

$$\vec{E}_k = \cos(kx + \phi_k) + \cos(-kx + \phi_k - \pi) =$$
$$= 2 * \cos(\phi_k)\cos(kx - \pi/2) =$$
$$2 * \cos(\phi_k)(\cos(kx)\cos(-\pi/2) - \sin(kx)\sin(-\pi/2))$$
$$= 2 * \cos(\phi_k)\sin(kx)$$
$$I = \sum_k 4\cos^2(\phi_k)\sin^2(kx) = \sum_k 4\cos^2(\phi_k)(1 - \cos^2(kx))$$

BACUS

N • E • W • S

Sponsorship Opportunities

Sign up now for the best sponsorship opportunities for Photomask 2011 and Advanced Lithography 2012. Contact:

Teresa Roles-Meier
Tel: +1 360 676 3290
teresar@spie.org

Advertise in the BACUS News!

The BACUS Newsletter is the premier publication serving the photomask industry. For information on how to advertise, contact:

Teresa Roles-Meier
Tel: +1 360 676 3290
teresar@spie.org

BACUS Corporate Members

Aprio Technologies, Inc.
ASML US, Inc.
Brion Technologies, Inc.
Coherent, Inc.
Corning Inc.
Gudeng Precision Industrial Co., Ltd.
Hamatech USA Inc.
Inko Industrial Corp.
JEOL USA Inc.
KLA-Tencor Corp.
Lasertec USA Inc.
Micronic Laser Systems AB
RSoft Design Group, Inc.
Synopsys, Inc.
Toppan Photomasks, Inc.

Industry Briefs

■ IBM demos cognitive computer chips (Source EE Times)

PORTLAND, Ore.—By replicating the functions of neurons, synapses, dendrites and axons in the brain using special-purpose silicon circuitry, IBM claims to have developed the first custom cognitive computing cores that bring together digital spiking neurons with ultra-dense, on-chip, crossbar synapses and event-driven communication.

The eventual goal is to create a brain-like 10 billion neuron, 100 trillion synapse cognitive computer with comparable size and power consumption to the human brain.??"We want to extend and complement the traditional von Neumann computer for real-time uncertain environments," said Dharmendra Modha, project leader for IBM Research. "Cognitive computers must integrate the inputs from multiple sensors in a context dependent fashion in order to close the real-time sensory-motor feedback loop." Though IBM claims its custom cognitive computing cores are the first of their kind, a rival European program using conventional ARM cores called SpiNNaker— for spiking neural network architecture—was announced last month.

■ Varian shareholders okay Applied acquisition

SAN FRANCISCO— Varian Semiconductor Equipment Associates Inc. said Friday (Aug. 12) that its shareholders approved of the proposed $4.9 billion acquisition of the firm by Applied Materials Inc.

Varian (Gloucester, Mass.) said the transaction was approved by holders of about 52.8 million shares of the company's outstanding common stock. Roughly 237,000 shares voted against the merger, Varian said.

"Varian said it continues to expect that the acquisition will be completed during the second half of this year. The closing of the merger is subject to the satisfaction or waiver of certain other closing conditions, including the approval of the U.S. Justice Dept., Varian said.

Applied and Varian announced in May that they signed a definitive agreement under which Applied would acquire Varian for $63 per share in cash for a total price of approximately $4.9 billion.

■ EUV delay will slow NAND supply growth

SANTA CLARA, Calif. – Delays delivering next-generation lithography will slow the growth in supply of NAND flash, said the chief technologist of SanDisk in a keynote address at the Flash Memory Summit here. In an otherwise upbeat assessment of the outlook for the flash market, Yoram Cedar waved a yellow flag about delays fielding extreme ultraviolet lithography. The lack of EUV tools will result in the historical increases in flash supply and decreases in cost to be more moderate with future process technologies, he said. Existing immersion lithography tools will serve flash makers down to geometries of less than 10nm, two generations from today's processes, he said. In addition, vendors are working to create 3-D stacks of NAND strings using existing fab tools to further boost capacity and supply, he added. Further in the future, chip makers including SanDisk are developing 3-D structures that use changes in resistance to create denser chips. But the so-called resistive RAM will require EUV tools, he said. Cedar declined to give any specifics about the timeframe for EUV or the status of the current 3-D chip research. However, he did say chip makers expect to ship 64 and 128 Gbit flash devices using immersion tools. "Many people in the semiconductor industry are very concerned about EUV not only from the standpoint of its availability but also its cost—these things will cost many millions of dollars," said one audience member in question to Cedar after the keynote.

Some pre-production EUV tools reportedly began shipping in January. Costs for the tools could soar as high as $120 million, according.

Cedar expressed optimism that EUV systems will be affordable. He also noted historical fears of an end to Moore's Law have so far been unfounded.

"When we were at 90nm, we thought 56nm was difficult and may be the end of the game," he said. The good news is flash demand is broad and strong. Flash is expected to grow 25 percent on a compound basis through 2015, nearly double the rate of hard disk storage and far above DRAM at only one percent, he said. About a third of all NAND bits will go to smart phones by 2015 when as many as 1.1 billion units ship, Cedar said. Tablets will take another 15 percent of NAND bits for 327 million systems that year, he added. "Tablets represent a sizeable market that came from nowhere," he said. "There is so much new development here that wasn't forecast three or four years ago, and there's no reason this will not continue," he added. He projected solid-state drives will consume 25 percent of NAND bits, selling into 133 million units for clients and 12 million for servers. The rest of NAND supply, about 26 percent, will go into existing systems such as MP3 players, USB drives and digital cameras, he said.

Join the premier professional organization for mask makers and mask users!

About the BACUS Group

Founded in 1980 by a group of chrome blank users wanting a single voice to interact with suppliers, BACUS has grown to become the largest and most widely known forum for the exchange of technical information of interest to photomask and reticle makers. BACUS joined SPIE in January of 1991 to expand the exchange of information with mask makers around the world.

The group sponsors an informative monthly meeting and newsletter, BACUS News. The BACUS annual Photomask Technology Symposium covers photomask technology, photomask processes, lithography, materials and resists, phase shift masks, inspection and repair, metrology, and quality and manufacturing management.

Individual Membership Benefits include:

- Subscription to BACUS News (monthly)
- Complimentary Subscription *Semiconductor International* magazine
- Eligibility to hold office on BACUS Steering Committee

spie.org/bacushome

Corporate Membership Benefits include:

- Three Voting Members in the SPIE General Membership
- Subscription to BACUS News (monthly)
- One online SPIE Journal Subscription
- Listed as a Corporate Member in the BACUS Monthly Newsletter

spie.org/bacushome

Calendar

2011

SPIE Photomask Technology

19-22 September 2011
Monterey Marriott
and Monterey Conference Center
Monterey, California, USA
spie.org/pm

2012

Advanced Lithography

12-16 February 2012
San Jose Convention Center and San Jose Marriott
San Jose, California, USA
spie.org/alcall

Submit your Abstracts Now!

SPIE Photomask Technology

10-13 September 2012
Monterey Marriott and Monterey Conference Center
Monterey, California, USA
spie.org/pm

You are invited to submit events of interest for this calendar. Please send to lindad@spie.org; alternatively, email or fax to SPIE.

SPIE is an international society advancing light-based technologies.

International Headquarters
P.O. Box 10, Bellingham, WA 98227-0010 USA
Tel: +1 888 504 8171 or +1 360 676 3290
Fax: +1 360 647 1445
help@spie.org • SPIE.org

Shipping Address
1000 20th St., Bellingham, WA 98225-6705 USA

SPIE Europe
2 Alexandra Gate, Ffordd Pengam, Cardiff, CF24 2SA, UK
Tel: +44 29 2089 4747
Fax: +44 29 2089 4750
spieeurope@spieeurope.org • www.spieeurope.org